Precision Optical Light Curves of LEO and GEO Objects

Paul Chote, James A. Blake, Don Pollacco
Astronomy & Astrophysics Group, University of Warwick, UK

ABSTRACT

Optical light curves are becoming an essential tool for classifying and characterising the properties of resident space objects. The intensity and colour of reflected sunlight probes the structure and reflectivity of the object, which evolves on a range of timescales due to changes in the objects attitude and the observer-object-sun geometry. Light curves therefore encode a signature of the object's structure and rotational properties, which can be analysed to constrain properties of the objects or applied en-masse to classify unknown objects via machine learning techniques.

A new research group has formed at the University of Warwick with a goal of studying the characteristics and dynamics of man-made objects orbiting the Earth. Here we describe two prototype robotic surveys that we are undertaking to obtain high-cadence, precisely calibrated light curves for objects in both LEO and GEO regimes.

LEO light curves are being obtained for relatively bright (Gaia $G_{BP} < 10$) targets using the SuperWASP telescope, which has been reconfigured with a ~ 200 deg^2 field of view and GPS-based timing. Targets are observed as streaks in sidereally tracked images that tile $\sim 70\,\%$ of the pass across the sky, and a custom reduction pipeline extracts light curves with an effective time cadence $\lesssim 100$ ms that are calibrated against the Gaia catalogue.

The GEO survey uses a temporarily installed 14" f/2.2 telescope and similar observing techniques to obtain a short ($\sim$30 minute) first-pass classification light curve at a < 1 s effective cadence to characterise the short-period variability of geosynchronous objects.

We provide an overview of the survey strategies and analysis and present some example results obtained during the first month of operations.

1. INTRODUCTION

Dramatic improvements in launch technologies and cost are driving a rapid expansion in the commercial use of space. The increased utilisation of the near-earth orbital environment brings the need for much greater confidence and understanding of the position and dynamics of the resident population. This is particularly important for the large and growing population of defunct satellites and debris objects that are not actively controlled, and therefore pose hazards that must be actively avoided.

In order to understand, and eventually remove, these objects it is important to measure and understand their rotational dynamics. The vast majority of objects are too small to directly image, so most observational techniques are limited to detecting integrated light. Optical light curves provide a running measure of the object's brightness with time, which varies as the illuminated face of the object presented to the observer changes.

Objects that are not actively stabilised will begin to tumble under the influence of various external torques [see e.g. 1, 2], which are still poorly understood. The tumbling motion creates a periodic signal (or signals) in the observed light curve that traces the phase of the rotation. Many studies [e.g. 3, 4, 5, 6, 7] have been done over the years to measure tumbling rates (which are typically of the order of seconds to minutes) and track how they change with time, but these have covered only a small fraction of the total population. Actively stabilised geostationary satellites will show variability over longer timescales as the solar phase angle varies the illuminated face of the satellite.

While coarse measurements can reveal periodic signals that constrain the gross rotational properties of a target, more precise and higher cadence observations can reveal finer details that can, in theory, be matched to specific models of the target geometry [e.g. 8, 9] to identify the specific attitude or to infer its shape and properties. For example, the presence (or absence) of sharp glints can indicate whether the target has flat reflective surfaces, and can constrain the

rotation rate [10]. Observations in multiple colours [e.g. 11, 12, 13] or time-resolved spectroscopy [e.g. 14, 15] can reveal information about the materials from which the object is composed.

A key limitation in developing our understanding of the photometric properties of space objects is the requirement to obtain more, and higher quality photometric observations for a range of objects. Here, we describe two surveys that are currently underway to measure high-cadence, photometrically calibrated light curves for a large number of objects in both LEO and GEO regimes. These data sets will be used as a basis for future studies into machine learning classification of light curves, population statistics, and targeted studies to attempt to model the dynamics and photometric signatures of specific objects.

2. INSTRUMENTATION AND OBSERVATION STRATEGY

Observations are being obtained using two robotic telescopes, shown in Fig. 1, which are part of the University of Warwick's facilities within the Roque de Los Muchachos observatory on La Palma in the Canary Islands.

Fig. 1: SuperWASP North (left) and the temporarily installed RASA 36 cm telescope (right) at the Roque de los Muchachos Observatory.

2.1 SuperWASP

The LEO survey is making use of the SuperWASP North telescope [16]. SuperWASP North (hereafter SuperWASP) and its sister facility in South Africa (SuperWASP South) conducted what is to date the most successful ground-based exoplanet survey, discovering nearly 200 confirmed Hot Jupiter class planets between 2004 – 2018.

The SuperWASP design features an equatorial telescope mount holding an array of 8 co-mounted 200 mm f1.8 camera lenses. Each lens is paired with a 2k×2k back-illuminated CCD, imaging a field of view of $8^\circ \times 8^\circ$ with a plate scale of 14 arcseconds per pixel. The LEO survey uses six of the cameras arranged in a 16° diameter field of view, with overlap to allow simultaneous observations in at least two cameras over much of the field. A broad-band filter covering approximately $400 - 700\,\mathrm{nm}$ is installed in each lens. This is a close match to the G_{BP} band-pass of the *Gaia* survey [17], which provides an excellent catalogue for both photometric and astrometric calibration.

SuperWASP has been upgraded with an external timing and control system based on a *Raspberry Pi* single-board computer and a custom add-on board that includes a pulse generator and GPS timing module. The system sits conceptually on top of the original telescope control systems, issuing commands for the mount via `ssh` and triggering simultaneous exposures by sending GPS-timestamped trigger pulses to the cameras. This timing solution is based on the principles of an earlier time-series photometer instrument, *Puoko-nui* [18].

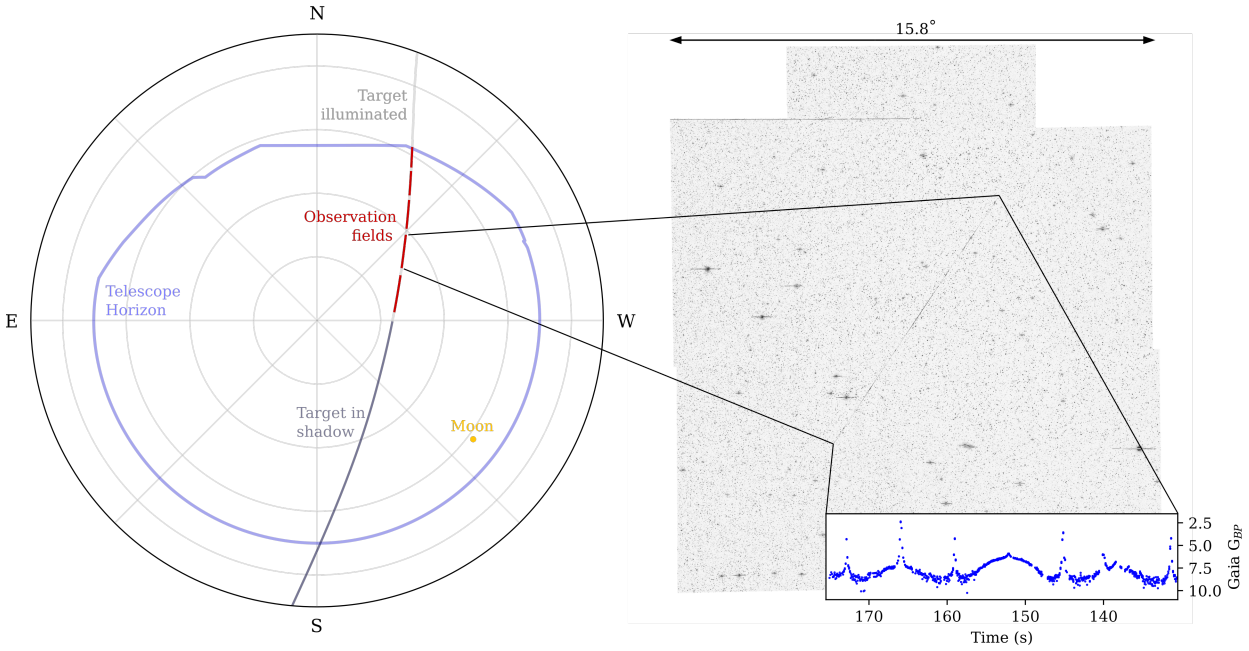

Fig. 2: A schematic illustration of the LEO observation procedure using SuperWASP. Left: The pass of the target across the sky is divided into a series of fields that account for the visibility limits of the telescope, shadow cone of the Earth, separation from the Moon, and dead time while the telescope slews and cameras read out. Right: The footprint of a single pointing (shown as a mosaic of the 6 cameras) captures a tumbling satellite as it streaks across the field. Photometry is extracted from the streak with an effective time resolution set by the speed of the target across the CCDs.

LEO passes are observed by slewing the mount to a series of pre-calculated fields and taking images that are timed to start just after the target enters the field of view of the camera array. Exposures end either just before the target leaves the field of view, or once a maximum exposure time of 45 seconds (chosen to reduce the amount of background flux from blended stars) has elapsed. The cameras read out while the mount slews to the next field, and the process repeats until the target sets below the visible horizon or disappears into the Earth's shadow. This procedure is illustrated in Fig. 2.

The fields in each pass are repeated to obtain reference images that allow the blended flux from background stars to be measured and subtracted from the light curve. The reference images are taken immediately after each pass to minimise any systematic effects due to changes in airmass, seeing, and mount orientation.

2.2 RASA

A 36 cm Rowe-Ackermann Schmidt Astrograph (RASA) paired with a FLI ML50100 camera has been temporarily installed on a Paramount ME mount for the duration of the GEO survey. Robotic control software has been adapted from the *Warwick 1 metre* (W1m) telescope, which is also based on La Palma. A custom GPS timestamping unit connected to the camera measures precise exposure start and end times.

The system provides a field of view of $3.6^\circ \times 2.7^\circ$ with a platescale of 1.6 arcsecond per pixel. Observations are made in white light, and matched to the *Gaia* G band-pass for photometric calibration.

GEO objects can be observed in one of several modes (non-tracking, sidereal tracking, object tracking), but for our initial survey all objects are observed using the sidereal tracking rate, which fixes the background stars as point sources and trails the target across the CCD at ~ 15 arcsec / sec (~ 0.1 s / px). CCD readout dead time and storage requirements are reduced by windowing the CCD to a $3.7^\circ \times 0.9^\circ$ strip. Data is acquired using 10 s exposures, with approximately 2 s readout dead time between exposures.

The robotic control software automatically acquires the target on one edge of the CCD and collects images as it drifts across the field of view. It adjusts its pointing once the target reaches the opposite edge of the field, and repeats until sufficient data is collected. Each target is observed for 30 minutes as a trade off between capturing at least one rotation

cycle for the majority of tumbling objects versus maximising the number of objects that can be observed during the limited (7 week) survey campaign.

Separate reference exposures are not required because the relatively slow drift rates at GEO mean that the same star fields are observed for many tens of exposures. The previous (or next, for the first exposure) exposure in the sequence can be used as a reference to measure the background flux in each aperture.

3. TARGET SELECTION AND PLANNING

Targets lists are generated each night by querying relatively recent (< 7 day old) LEO and GEO TLEs from the Space-Track web API. These are filtered to a short list of candidates based on object visibility above the horizon, the Earth's shadow cone, and separation from the moon.

Observation planning for SuperWASP is complicated by the physical constraints of its enclosure, which imposes severe visibility limits towards the north and to a lesser extent the south. These limitations are reduced by observing fields to the north (south) with the southern-most (northern-most) camera in the array, which is lifted above the declination axis of the telescope, gaining an extra 10 – 20 degrees of sky visibility while the rest of the array is occulted by the walls.

Fields are scheduled using a simple brute-force algorithm that calculates the first time/position where the target is visible, then steps forward in time until it has moved by the diameter of the field of view (minus a safety margin to allow for errors in the TLE and telescope pointing). The average of the start and end coordinates defines the RA and Dec for the field. A dead time of 15 s is added to allow the cameras to read out and the mount to slew to the next field, and the process is repeated until the target sets, moves into shadow, or moves within 30 degrees of the Moon.

Candidate observations are scheduled using an algorithm that prioritises nominated targets, followed by targets that are visible for between 5 and 10 minutes, then attempts to fill the remaining gaps in a way that minimises idle time.

Observations for the RASA are much simpler to schedule because the relatively small movement of GEO objects on the sky allows most objects to be observed at any time of the night. The main additional constraint is to avoid the galactic plane, where the large background star density makes the astrometric calibration difficult and causes significant problems with background star blending. Targets are scheduled in blocks from the start of the night, selecting the target with the best solar phase angle that has not yet been observed. Repeat observations are made if no new targets are available to observe.

4. DATA REDUCTION

Reduction pipelines have been developed to extract calibrated photometry along streaks in sidereally tracked SuperWASP and RASA frames. The pipelines are written in Python 3, and leverage a number of open source astronomical tools and Python packages including `Astrometry.net` [19], `Astropy` [20, 21], `HOTPANTS` [22], `Matplotlib` [23], `SEP` [24], `SExtractor` [25], `Skyfield` [26], `SWarp` [27] and `photutils` [28].

The key steps in the reduction are outlined graphically in Fig. 3. The raw target and reference images are first processed by applying standard bias and flat field corrections (A, B, C), and an initial astrometric fit is obtained. The astrometric solution for the SuperWASP frames is then refined by fitting a custom 2D distortion map, which is required as `Astrometry.net` cannot reliably fit the strong barrel distortion present in these images.

Reference stars for each frame are queried from the *Gaia* DR2 catalog [29], and filtered to reject stars that are blended on the image pixel scale. These are cross-matched to the sources detected by the astrometric solution, and the difference between the catalog and instrumental magnitudes allow a Gaia G_{BP} (SuperWASP) or Gaia G (RASA) zero point to be calculated for each frame.

The SuperWASP images for each pointing are combined into a difference-image mosaic by registering and subtracting the reference images from each camera from the corresponding target image, then resampling and combining the results to create a mosaic of the full field of view. These difference images remove most of the stars, leaving the target trail visible in a form that is more amenable to both automated and manual detection of faint trails. This step has not yet been required for the RASA images, as the short GEO streaks and improved pixel scale have less blending problems and are more tractable to standard astronomical source detection algorithms.

The trail predicted by the TLE may be offset from the observed streaks by many pixels (D) due to the precision limitations and propagation errors, and must be refined to match the observations (E). This is currently achieved manually by having the user mark the ends of the trail in each footprint image, then applying a χ^2 minimisation to adjust the TLE parameters to achieve a closer match.

The refined TLE is used to place rectangular apertures along the trail in the target (F) and reference (G) images, and the apparent magnitude of the target is calculated from the difference in integrated fluxes, accounting for the relative zero points in the two images and the time spent in each aperture. The width of the apertures is set by the point-spread function of the instrument and the accuracy of the cross-track TLE fit. The length of the aperture along the trail is set by the desired effective time resolution and signal to noise ratio for the extracted light curve.

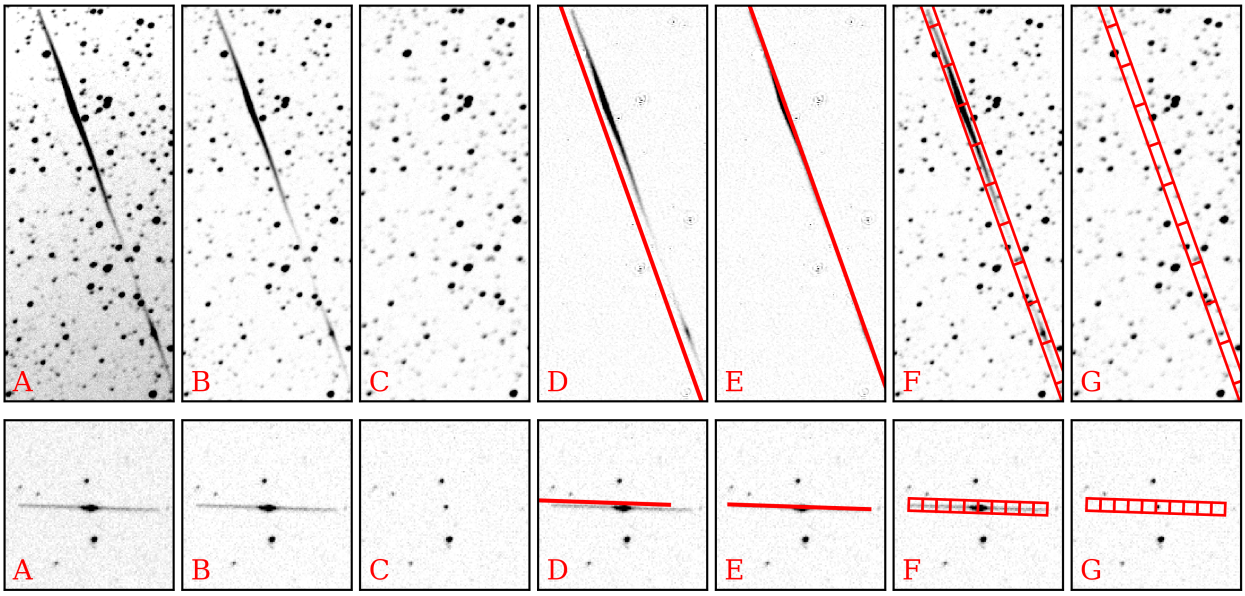

Fig. 3: Sub-windows of SuperWASP (top) and RASA (bottom) images demonstrate the main steps in our streak photometry pipeline. The trail shown covers approximately 10 s of the pass of a tumbling LEO (top) and GEO (bottom) satellite. (A) Raw target exposure; (B) Calibrated target exposure; (C) Calibrated reference exposure; (D) TLE streak position; (E) Fitted streak position; (F) Target apertures using 1s extraction cadence; (G) Reference apertures. See text for further detail.

5. SURVEY PROGRESS AND FUTURE WORK

Initial prototyping for the instrumentation and observation strategy was carried out in late 2018 and early 2019. Robotic observations began in July 2019, with the RASA survey ending in late August 2019 and SuperWASP continuing for the next several months.

The majority of observations are being archived for future reduction, as the data collection rate currently outpaces our ability to extract light curves. This is partly caused by computing limitations, and the requirement for manual input to align the TLE and observed streak positions. Work is currently underway to develop an automated technique that can robustly fit trails featuring strong brightness variations from tumbling and glinting objects, and we expect to upgrade our computing infrastructure in the near future.

More than 1600 light curves were obtained in the first seven weeks of operations covering more than 350 GEO objects using the RASA and 550 LEO targets using SuperWASP.

Figure 4 demonstrates a sample of light curves of LEO objects that have been obtained using SuperWASP. As expected we find objects with a range of light curve morphologies, from featureless through slow variations, to dramatic short-period periodic or non-periodic variability. For bright objects ($G_{BP} \lesssim 6$) photometric precision is of the order of a few percent at ~ 100 ms time resolution, which can be improved by binning the data in the time domain. We find that

we can obtain useful data for -1 $\lesssim G_{BP} \lesssim$ 10; fainter objects become sky and instrument noise limited, and brighter objects saturate the CCD. We note, however, that the specific precision and saturation thresholds depend on the altitude of the target - objects in higher orbits move with a lower angular speed, meaning the object spends more time in each CCD pixel, producing a higher signal at the same apparent brightness. The environmental conditions and background star density are also important factors in the resulting precision.

This brightness threshold means that we are not able to observe the faint end of the LEO population. We attempt to compensate for this by limiting observations to objects with `RCS_SIZE = LARGE` in the Space Track database.

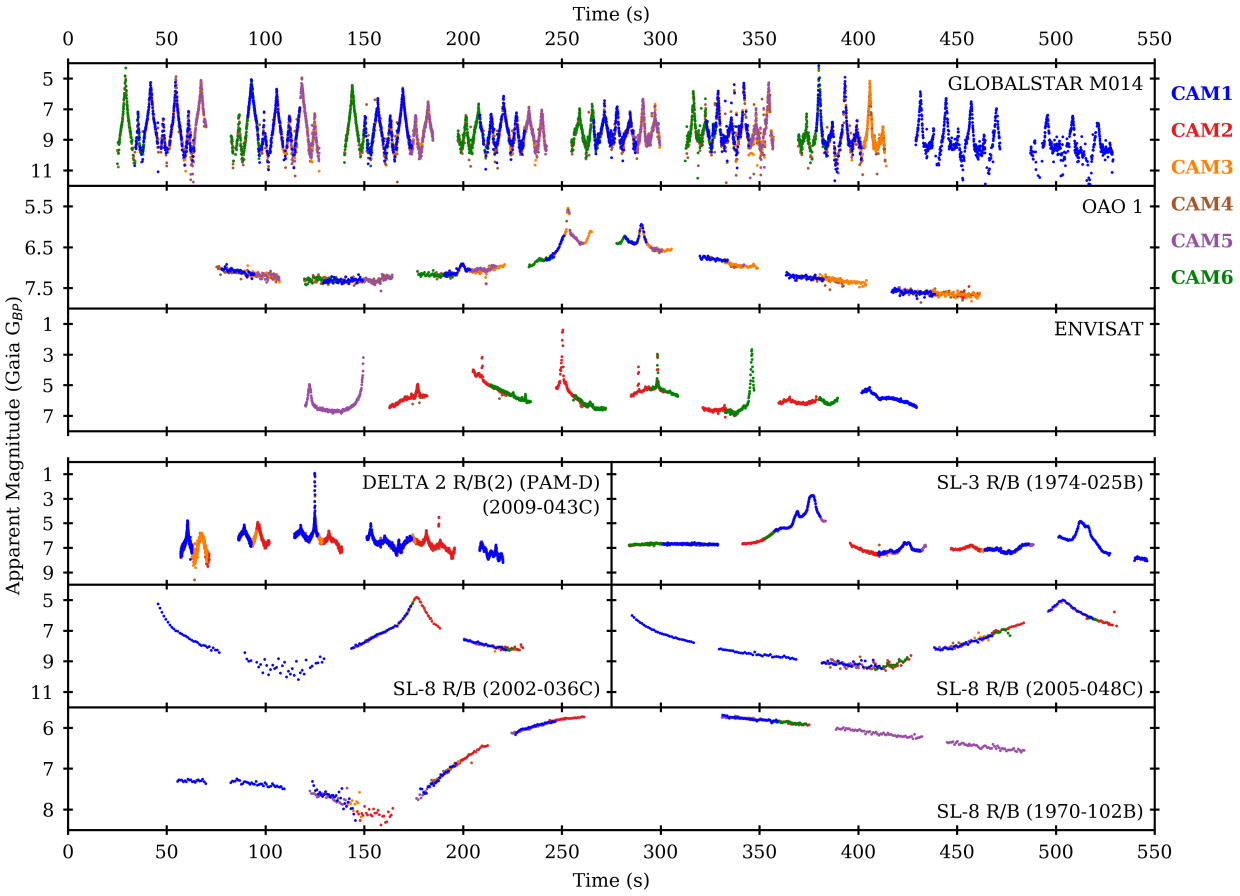

Fig. 4: Example light curves of LEO satellites (top) and rocket bodies (bottom) obtained with SuperWASP. Photometric points are color-coded by camera according to the legend on the right. Glints and smoother brightness variations are visible over a range of timescales. The regular gaps in the light curves are due to the dead time while the telescope moves between fields.

The LEO light curve database will form the basis for an EOARD-funded PhD project starting in September 2019, which will focus on the applications of machine learning techniques to the classification of LEO objects from their optical light curve properties.

Figure 5 demonstrates phase-folded light curves for several GEO objects obtained with the RASA. We obtain photometric precision of a few percent within 1 second at G $\sim$ 14, but can obtain significantly better precision at higher cadences by phase folding the light curves. This improvement can be seen by comparing the blue and grey points in the examples shown.

We expect that a significant fraction of the GEO light curves (corresponding to satellites with active 3-axis stabilisation) will not show significant features over the 30 minute observation window, and a smaller fraction will be too faint to extract useful data from the $\sim$ 0.1 s/px streaked frames. These targets will be identified and followed up in future surveys that use more appropriate observational strategies. Repeat epochs are planned to be able to track the evolution

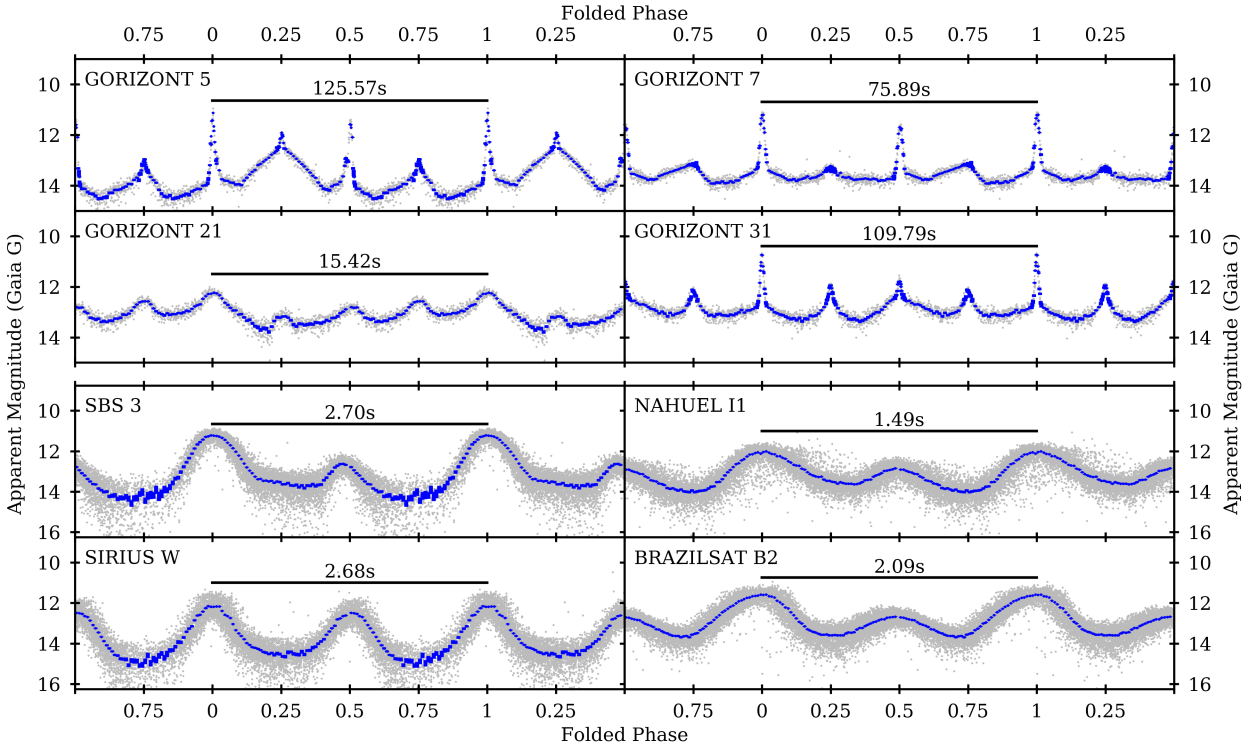

Fig. 5: Folded GEO light curves illustrating the photometric signature of several satellites based on the KAUR-3 (top) and HS376 (bottom) busses. Raw photometry is shown in grey, and phase-binned measurements (with 1-sigma errors) in blue. The Gorizont satellites are found to feature broadly similar four-peaked rotation profiles, but the finer details and periods differ between objects. The HS376-based satellite observations demonstrate the ability to measure very short periods, but the point-spread function of the telescope acts to blur the shape of sharp features that occur on timescales $\lesssim 0.5\,\mathrm{s}$.

of rotation periods for the sample over time.

Several studies are planned for the GEO light curve database, including (a) searching for trends in the rotation period vs age for different satellite busses to investigate the YORP effect, (b) searching for trends in the rotational profiles that may be used to identify the bus type of an unknown object, (c) investigating the relationship between glint properties and rotation period for different satellite busses.

Our observational ambitions include expanding our capabilities for multi-colour photometry, first by installing filters in SuperWASP and later by deploying a dual-RASA system with synchronised cameras and different filters in each tube.

6. SUMMARY

We have developed two robotic surveys to obtain calibrated high-cadence light curves for objects in the LEO and GEO regimes. We have described our instrumentation, observational procedures, and reduction pipelines. Examples demonstrating the capabilities of our approach are shown. Data collection is currently ongoing, with reduction and analysis to begin in earnest later in 2019.

7. REFERENCES

[1] A. A. Albuja, D. J. Scheeres, and J. W. McMahon. Evolution of angular velocity for defunct satellites as a result of YORP: An initial study. *Advances in Space Research*, 56:237–251, July 2015.

[2] A. A. Albuja et al. The YORP effect on the GOES 8 and GOES 10 satellites: A case study. *Advances in Space Research*, 61(1):122–144, 2018.

[3] P. Papushev, Y. Karavaev, and M. Mishina. Investigations of the evolution of optical characteristics and dynamics of proper rotation of uncontrolled geostationary artificial satellites. *Advances in Space Research*, 43(9):1416–1422, 2009.

[4] C. R. Binz, M. A. Davis, B. E. Kelm, and C. I. Moore. Optical survey of the tumble rates of retired GEO satellites. Technical report, Naval Research Lab Washington DC, 2014.

[5] R. L. Cognion. Rotation Rates of Inactive Satellites Near Geosynchronous Earth Orbit. In *Proceedings of the Advanced Maui Optical and Space Surveillance Technologies Conference*, 2014.

[6] W. Ryan and E. Ryan. Photometric Studies of Rapidly Spinning Decommissioned GEO Satellites. In *Advanced Maui Optical and Space Surveillance Technologies Conference*, page 93, 2015.

[7] Jiří Šilha, Jean-Noël Pittet, Michal Hamara, and Thomas Schildknecht. Apparent rotation properties of space debris extracted from photometric measurements. *Advances in Space Research*, 61(3):844 – 861, 2018.

[8] Jiri Silha, Thomas Schildknecht, Jean-Nöel Pittet, Dominik Bodenmann, Ronny Kanzler, P Karrang, and Holger Krag. Comparison of envisats attitude simulation and real optical and slr observations in order to refine the satellite attitude model. In *Proceedings of AMOS Conference, Maui, Hawaii*, pages 7651–7657, 2016.

[9] Michael A. Earl, Philip W. Somers, Konstantin Kabin, Donald Bédard, and Gregg A. Wade. Estimating the spin axis orientation of the Echostar-2 box-wing geosynchronous satellite. *Advances in Space Research*, 61(8):2135–2146, Apr 2018.

[10] J. C. Hinks and J. L. Crassidis. Angular velocity bounds via light curve glint duration. In *AIAA Guidance, Navigation, and Control Conference*, page 0627, 2016.

[11] T. Cardona et al. BVRI photometric observations and light-curve analysis of GEO objects. *Advances in Space Research*, 58(4):514–527, 2016.

[12] Y. Lu, C. Zhang, R.-y. Sun, C.-y. Zhao, and J.-n. Xiong. Investigations of associated multi-band observations for GEO space debris. *Advances in Space Research*, 59:2501–2511, May 2017.

[13] Emiliano Cordelli, Peter Schlatter, and Thomas Schildknecht. Simultaneous multi-filter photometric characterization of space debris at the swiss optical ground station and geodynamics observatory zimmerwald. In *Advanced Maui Optical and Space Surveillance Technologies Conference (AMOS)*, 2018.

[14] D. Bédard and G. A. Wade. Time-resolved visible/near-infrared spectrometric observations of the Galaxy 11 geostationary satellite. *Advances in Space Research*, 59:212–229, January 2017.

[15] A. Vananti, T. Schildknecht, and H. Krag. Reflectance spectroscopy characterization of space debris. *Advances in Space Research*, 59:2488–2500, May 2017.

[16] D. L. Pollacco, I. Skillen, A. Collier Cameron, D. J. Christian, C. Hellier, J. Irwin, T. A. Lister, R. A. Street, R. G. West, D. R. Anderson, W. I. Clarkson, H. Deeg, B. Enoch, A. Evans, A. Fitzsimmons, C. A. Haswell, S. Hodgkin, K. Horne, S. R. Kane, F. P. Keenan, P. F. L. Maxted, A. J. Norton, J. Osborne, N. R. Parley, R. S. I. Ryans, B. Smalley, P. J. Wheatley, and D. M. Wilson. The WASP Project and the SuperWASP Cameras. *pasp*, 118:1407–1418, October 2006.

[17] Gaia Collaboration, T. Prusti, J. H. J. de Bruijne, A. G. A. Brown, A. Vallenari, C. Babusiaux, C. A. L. Bailer-Jones, U. Bastian, M. Biermann, D. W. Evans, and et al. The Gaia mission. *Astronomy & Astrophysics*, 595:A1, November 2016.

[18] P. Chote, D. J. Sullivan, R. Brown, S. T. Harrold, D. E. Winget, and D. W. Chandler. Puoko-nui: a flexible high-speed photometric system. *Monthly Notices of the Royal Astronomical Society*, March 2014.

[19] D. Lang et al. Astrometry.net: Blind astrometric calibration of arbitrary astronomical images. *The Astronomical Journal*, 139(5):1782, 2010.

[20] T. P. Robitaille et al. Astropy: A community Python package for astronomy. *Astronomy & Astrophysics*, 558:A33, 2013.

[21] A. M. Price-Whelan et al. The astropy project: building an open-science project and status of the v2.0 core package. *The Astronomical Journal*, 156(3):123, 2018.

[22] A. Becker. HOTPANTS: High Order Transform of PSF ANd Template Subtraction. Astrophysics Source Code Library, April 2015.

[23] J. D. Hunter. Matplotlib: A 2d graphics environment. *Computing in Science & Engineering*, 9(3):90–95, 2007.

[24] K. Barbary. SEP: Source Extractor as a library. *The Journal of Open Source Software*, 1(6):59, 2016.

[25] E. Bertin and S. Arnouts. SExtractor: Software for source extraction. *Astronomy and Astrophysics Supplement Series*, 117(2):393–404, 1996.

[26] Skyfield. `http://rhodesmill.org/skyfield/`.

[27] E. Bertin, Y. Mellier, M. Radovich, G. Missonnier, P. Didelon, and B. Morin. The TERAPIX Pipeline. In D. A. Bohlender, D. Durand, and T. H. Handley, editors, *Astronomical Data Analysis Software and Systems XI*, volume 281 of *Astronomical Society of the Pacific Conference Series*, page 228, 2002.

[28] Larry Bradley, Brigitta Sipocz, Thomas Robitaille, Erik Tollerud, Z Vincius, Christoph Deil, Kyle Barbary, Hans Moritz Gnther, Mihai Cara, Ivo Busko, Simon Conseil, Michael Droettboom, Azalee Bostroem, E. M. Bray, Lars Andersen Bratholm, Tom Wilson, Matt Craig, Geert Barentsen, Sergio Pascual, Axel Donath, Johnny Greco, Gabriel Perren, P. L. Lim, and Wolfgang Kerzendorf. astropy/photutils: v0.6, January 2019.

[29] Gaia Collaboration, A. G. A. Brown, A. Vallenari, T. Prusti, J. H. J. de Bruijne, C. Babusiaux, and C. A. L. Bailer-Jones. Gaia Data Release 2. Summary of the contents and survey properties. *ArXiv e-prints*, April 2018.